An Isolated Helix Persists in a Sparsely Populated Form of KIX under Native Conditions†

Martin Tollinger,*,‡ Karin Kloiber,‡ Bianka Ágoston,‡ Cornelia Dorigoni,‡ Roman Lichtenecker,§ Walther Schmid,§ and Robert Konrat‡

Department of Biomolecular Structural Chemistry, University of Vienna, Campus Vienna Biocenter 5, A-1030 Vienna, Austria, and Institute of Organic Chemistry, University of Vienna, Währinger Strasse 38, A-1090 Vienna, Austria

Received April 15, 2006; Revised Manuscript Received May 24, 2006

ABSTRACT: NMR relaxation dispersion techniques were used to investigate conformational exchange of the three-helix bundle protein KIX under native conditions. These experiments provide site-resolved kinetic information about microsecond-to-millisecond time scale motions along with structural (chemical shift) information without requiring a perturbation of the equilibrium. All kinetic data are consistent with an apparent two-state transition between natively folded KIX and a partially unfolded high-energy state that is populated to 3.0 ± 0.2% at 27 °C. By combining ^{13}C- and ^{15}N-based experiments that probe specific structural aspects, we show that the sparsely populated high-energy state displays a strong conformational preference. An isolated secondary structural element, C-terminal helix α3, is highly populated, while the hydrophobic core of the domain and the remainder of the protein backbone, including helices α1 and α2, are disordered and devoid of specific interactions. This high-energy state presumably represents the equilibrium analogue of a folding intermediate that is transiently populated in stopped-flow kinetic experiments [Horng, J. C., Tracz, S. M., Lumb, K. J., and Raleigh, D. P. (2002) *Biochemistry 44*, 627−634].

A comprehensive description of how a protein folds requires the detailed structural characterization of its unfolded state along with any partially unfolded states that may be transiently populated during the folding transition. Unfolded and partially unfolded states of proteins represent ensembles of rapidly interconverting and structurally heterogeneous conformations that can display variable amounts of residual structure and compactness (*1*−*3*). The exact composition of these states appears, however, to be highly sensitive to experimental (solvent) conditions, and quite generally, chemical denaturing agents and experimental conditions that promote unfolding lead to loss of residual structure and compactness (*1*).

In light of the sensitivity of (partially) unfolded proteins to experimental conditions, kinetic and structural studies by methods that do not require a perturbation of the folding equilibrium are crucial. For most natively folded proteins, however, such states are notoriously difficult to study due to their low population at equilibrium. With the exception of hydrogen exchange methods (*4*, *5*), most experimental approaches require tipping of the balance between native ground states and high-energy states in populating unfolded and partially unfolded forms of proteins, for example, by chemical modifications of side chains, by removal of cofactors, or by means of mutation (*6*−*8*). Only in few cases are these states sufficiently populated under native conditions to permit direct structural characterization by standard NMR[1] and other spectroscopic methods (*2*).

Protein folding kinetic measurements are typically performed by methods in which folding or unfolding is initiated by rapidly changing the experimental conditions such as denaturant concentration, temperature, or pH, and the recovery of equilibrium is monitored (*9*). Recently, NMR relaxation dispersion methods have become available, enabling protein folding studies under native conditions without requiring a perturbation of the folding equilibrium (*10*). Kinetic information about the folding and unfolding process, along with structural information and pathway information, has been obtained even in cases where unfolded states (and folding intermediates) are populated to only a few percent (*11*−*15*). Moreover, these experiments provide information at multiple sites within the protein, unlike spectroscopic techniques such as fluorescence and circular dichroism that provide nonspecific information about aromatic side chains and averaged properties of the polypeptide backbone, respectively.

In this work, we have studied microsecond-to-millisecond conformational exchange processes of the KID-binding (KIX) domain of CREB-binding protein (CBP). Like its paralogue, p300, CBP is a modular transcriptional coactivator that participates in the regulation of numerous

† This work was supported by grants from the WWTF (R.L., W.S., and R.K.) and the FWF (R.K. and K.K.). M.T. is a recipient of an E. Schrödinger Return Fellowship of the FWF.

* To whom correspondence should be addressed. Phone: +43 1 4277 52263. Fax: +43 1 4277 9522. E-mail: martin.tollinger@univie.ac.at.

‡ Department of Biomolecular Structural Chemistry.

§ Institute of Organic Chemistry.

[1] Abbreviations: NMR, nuclear magnetic resonance; CPMG, Carr−Purcell−Meiboom−Gill; CBP, CREB-binding protein; CREB, cyclic AMP response element-binding protein; KID, kinase-inducible transcriptional activation domain; KIX, KID-binding domain; NHX, native-state hydrogen exchange.

10.1021/bi0607305 CCC: $33.50
Published on Web 06/28/2006

transcriptional processes (*16*, *17*). In detail, the KIX domain of CBP is involved in the integration of signals from various signaling pathways in binding to a number of co-activators. The interaction domains of these co-activators are intrinsically unstructured in isolation but undergo folding on binding to KIX, underlining the prominent role of coupled folding and binding in the fine-tuning of protein−protein interactions (*18*). In addition, various interaction sites on the KIX domain have been identified (*19*−*22*), and the cooperativity of binding different interaction partners has been characterized in detail (*22*−*24*).

We have performed site-specific conformational exchange kinetic measurements by NMR relaxation dispersion techniques to investigate microsecond-to-millisecond processes in KIX under nondenaturing conditions. Specific structural aspects of conformational exchange were probed by combining backbone relaxation dispersion experiments in assessing secondary structure formation with side chain-based experiments in studying hydrophobic packing. All experimental data are consistent with an apparent two-state transition between natively folded KIX and a sparsely populated partially unfolded form. In the native state, KIX is composed of three α-helices (and two short 3_{10}-helices) that pack against each other and form an extended hydrophobic core (*19*, *22*). In the high-energy state of KIX, an isolated α-helix is retained and highly populated, while the bulk of the native structure, including the hydrophobic core, is disrupted.

MATERIALS AND METHODS

NMR Sample Preparation. His_6-KIX was prepared using the pHisKIX plasmid containing an N-terminal hexahistidine (His_6) tag and the CBP KIX coding region (residues 586−672) of KIX as described previously (*25*) but using BL21(DE3) *Escherichia coli* cells in M9 minimal medium containing $^{15}NH_4Cl$ as a nitrogen source. His_6-KIX was purified by Ni affinity chromatography followed by size exclusion chromatography. The His_6 tag was cleaved by incubation with thrombin, and KIX was purified to homogeneity by size exclusion chromatography. Two samples of KIX were employed in this study. The first was uniformly labeled with ^{15}N and protonated. The second sample was uniformly labeled with ^{15}N and selectively labeled with ^{13}C and ^{1}H at the C^{γ} methyls of Val residues and at C^{δ} methyl groups of Leu and Ile, while all other positions contained ^{12}C and ^{2}H (with the exception of exchange labile positions). [U-^{2}H,^{15}N], Ile-δ1-[$^{13}CH_3$], Leu-δ-,Val-γ-[$^{13}CH_3$/$^{12}C^{2}H_3$]KIX was prepared using D_2O-based media and [U-^{12}C,^{2}H]-D-glucose (2 g/L) as the main carbon source, $^{15}NH_4Cl$ as the nitrogen source, and 2-keto-3,3-$^{2}H_2$-4-^{13}C-butyrate (100 mg/L) and 2-keto-3-(methyl-$^{2}H_3$)-3-^{2}H-4-^{13}C-butyrate (120 mg/L) as amino acid precursors for Ile, Leu, and Val (*26*). Precursors were prepared in a non-stereospecific manner as described previously (*27*), and deuteration at position 3 of both compounds was achieved by exchange in D_2O at pH 12.6 for 5 h (*26*). Protein concentrations were determined from the absorbance at 280 nm, using an ϵ_{280} of 12 090 M^{-1} cm^{-1} as the extinction coefficient. Yields of 12−14 and 8 mg/L were obtained for ^{15}N-labeled KIX and selectively methyl-labeled KIX, respectively. NMR buffers contained 50 mM potassium phosphate (pH 5.5), 25 mM NaCl, 1 mM NaN_3, and a 92% H_2O/8% D_2O mixture. All experiments were performed at pH 5.5 to match conditions used in NMR structural studies of the KIX domain (*19*, *22*).

NMR Relaxation Dispersion Experiments. Backbone ^{15}N single-quantum (*28*, *29*) and side chain methyl ^{13}C single-quantum (*30*) relaxation dispersion experiments were performed on Varian Inova spectrometers operating at static magnetic field strengths of 11.7 and 18.8 T at 27 and 20 °C for ^{15}N-labeled KIX and selectively methyl-labeled KIX, respectively. CPMG-based radio frequency field strengths, ν_{CPMG}, ranged from 40 to 960 Hz (^{15}N) and from 33.3 to 1000 Hz (^{13}C), and relaxation delays of 50 and 60 ms for ^{15}N and ^{13}C, respectively, were used. Spectra were collected as series of two-dimensional data sets. Duplicate data sets were recorded at selected ν_{CPMG} values for error analysis. Protein concentrations were 1.0 mM for ^{15}N-labeled samples and 1.6 mM for the selectively methyl-labeled sample (unless stated otherwise). Peak intensities were converted to relaxation rates, and uncertainties in relaxation rates, σ, were calculated from repeat experiments as described previously (*12*).

Data Fitting. Conformational exchange involving KIX backbone ^{15}N and side chain methyl ^{13}C nuclei is in the intermediate to slow regime (depending on chemical shift differences) on the NMR chemical shift time scale. To prevent systematic errors for relatively slowly exchanging residues (*29*), exact numerical solutions of the Bloch equations, including magnetization transfer effects due to chemical exchange (*31*), were fit to the relaxation dispersion data, using either a model of two-site exchange (G ↔ E) between the native (folded) ground state (G) and an excited state (E), or three-site exchange models involving an additional (excited) state (see below). Least-squares fits were performed by adjusting exchange parameters to minimize the residual $\chi^2 = \sum(R_{2,\mathrm{eff}}^{\mathrm{exp}} - R_{2,\mathrm{eff}}^{\mathrm{calc}})^2/\sigma^2$, where $R_{2,\mathrm{eff}}^{\mathrm{exp}}$ and $R_{2,\mathrm{eff}}^{\mathrm{calc}}$ are the experimental and calculated relaxation rates, respectively, and the sum extends over all measurements included in the fit.

Relaxation dispersion profiles were fit to two-site exchange models in individual fits to yield site-specific values of k_{GE}, k_{EG}, and $|\Delta\omega_{fit}|$ and in global fits assuming uniform rate constants for the G → E and E → G transitions (k_{GE} and k_{EG}, respectively) but site-specific values of $|\Delta\omega_{fit}|$. Only relaxation dispersion profiles for which $\chi_{glob}^2/\chi_{ind}^2 < 1.5$ were retained for further analysis to exclude conformational fluctuations other than the global two-site G ↔ E transition. Experimental uncertainties in exchange parameters were estimated via a Monte Carlo approach (*32*) in which 100 synthetic data sets were generated using the exchange parameters obtained in the global fit along with the experimental error in rates (see above), and the global fit was repeated for all data sets. Errors quoted in the paper are standard deviations in fitted exchange parameters that were obtained in this procedure. Fits of the experimental data to three-state conformational exchange models were performed as described previously (*11*, *15*), and *F*-test statistic criteria (*32*) were used to assess the suitability of exchange models with more than two states.

Chemical Shifts. Only $|\Delta\omega_{fit}|$ values obtained from global fits are reported. Secondary chemical shifts, $\Delta\omega_{sec}$, were calculated as the difference between experimental and

random coil chemical shifts, which were determined using sequence-dependent correction factors for backbone ^{15}N (*33*) and tabulated random coil chemical shifts of Val, Leu, and Ile methyl ^{13}C nuclei (*34*).

Native-State Hydrogen Exchange and Urea Denaturation Experiments. A sample containing 100 μL of 3.1 mM ^{15}N-labeled KIX in ^{1}H potassium phosphate buffer [50 mM potassium phosphate (pH 5.5) and 25 mM NaCl] was diluted with 400 μL of 50 mM ^{2}H potassium phosphate buffer (pD 5.5) with 25 mM NaCl, and a series of ^{1}H$-^{15}$N heteronuclear single-quantum coherence (HSQC) spectra (duration of 13 min each, at 18.8 T and 27 °C) were collected starting after 2 min. ^{1}H$-^{2}$H exchange rate constants, k_{obs}, were determined by fitting the decay of peak volumes with time to a first-order exponential equation, and site-specific free energies were calculated using the relation $\Delta G = -RT \ln(k_{obs}/k_{int})$, where k_{int} is the intrinsic ^{1}H$-^{2}$H exchange rate (*35*).

Equilibrium urea denaturation experiments were performed to determine the free energy for complete unfolding of KIX using standard methods, by monitoring the circular dichroism signal at 222 nm (*36*). Buffers contained 50 mM potassium phosphate (pH 5.5), 25 mM NaCl, and 1 mM NaN_3, and the protein concentration was 10 μM. Urea concentrations were determined from the refractive index of each solution, and the denaturation data were fit to determine thermodynamic parameters as described previously (*37*). In addition, backbone ^{15}N single-quantum NMR relaxation dispersion experiments were performed at various concentrations (0.5, 1.0, and 1.5 M) of urea and with 50 mM potassium phosphate (pH 5.5), 25 mM NaCl, 1 mM NaN_3, and a 92% H_2O/8% D_2O mixture, at 27 °C. The protein concentration was kept at 1.0 mM for all experiments, and the data were analyzed as described above.

KIX Is Monomeric. Sedimentation equilibrium experiments have shown that KIX is monomeric in the micromolar concentration range (*21*). The rotational correlation time of KIX determined from ^{15}N relaxation parameters (R_1 and $R_{1\rho}$) employing standard NMR methodology (*38*, *39*) is invariant with protein concentration (between 0.7 and 1.8 mM) and consistent with values that are expected for an ~11 kDa protein, suggesting that KIX is also monomeric in the millimolar concentration range used for recording NMR data. This is further corroborated by the observation that backbone ^{15}N single-quantum relaxation dispersion experiments performed with 0.7 and 1.8 mM samples of KIX yielded values of k_{GE} and k_{EG} differing by <1 and <15 s^{-1}, respectively, from those of the 1.0 mM sample.

RESULTS

Figure 1 shows representative relaxation dispersion profiles for the backbone of KIX [^{15}N single-quantum (*28*, *29*)] and for side chain methyl groups [^{13}C single-quantum (*30*)]. For the majority of residues, conformational exchange on the microsecond-to-millisecond time scale contributes significantly to transverse relaxation rates, giving rise to sizable (nonflat) relaxation dispersion profiles. We carefully examined the experimental relaxation dispersion data to determine the exchange model that is appropriate for fitting the data and extracting information about the microsecond-to-millisecond conformational exchange process. Initially, ^{15}N relaxation dispersion profiles were fit for each site individually to a two-site exchange model (G ↔ E) to yield site-specific values of G → E and E → G rate constants (k_{GE} and k_{EG}, respectively), and site-specific differences in resonance frequencies between G and E states, $|\Delta\omega_{fit}|$, as well as χ_{ind}^2 residuals. Values of k_{GE} and k_{EG} obtained from individual fits are uniform to within 20% [$k_{GE} = 18 \pm 3$ s^{-1} and $k_{EG} = 580 \pm 130$ s^{-1} (excluding residues with very small exchange contributions, $R_{ex} < 3$ s^{-1} at 11.7 T, for which exchange parameters obtained from per-residue fits are inherently unreliable)], suggesting that all ^{15}N sites in KIX sense the same conformational transition. Subsequently, dispersion profiles for all sites (^{15}N) were fit collectively to a global two-site exchange model assuming uniform values of k_{GE} and k_{EG} for all residues but site-specific values of $|\Delta\omega_{fit}|$, along with χ_{glob}^2 residuals. Rate constants for ^{15}N-labeled KIX at 27 °C were determined: $k_{GE} = 17 \pm 1$ s^{-1} and $k_{EG} = 540 \pm 20$ s^{-1}, corresponding to a free energy difference between G and E states $\{\Delta G_{GE} = -RT \ln[(k_{GE})/(k_{EG})]\}$ of 2.1 ± 0.1 kcal/mol. For all 71 backbone amide resonances that are resolved in two-dimensional ^{1}H$-^{15}$N correlation spectra, $\chi_{glob}^2/\chi_{ind}^2 < 1.5$. Moreover, the small increase in χ^2 that was observed relative to individual fits (on average, $\chi_{glob}^2/\chi_{ind}^2 = 1.12$) is in accord with the reduction of the number of adjustable parameters in global fits at the 99% confidence level, which verifies that restraining rate constants to uniform values in a global fit is justified. The experimental relaxation dispersion data for all residues are therefore consistent with an apparent two-site conformational exchange model in which all sites experience identical kinetics.

To further verify the suitability of a two-state conformational exchange model in fitting the experimental data, relaxation dispersion profiles were fit to three-state models involving an additional state in linear (unconstrained, i.e.,

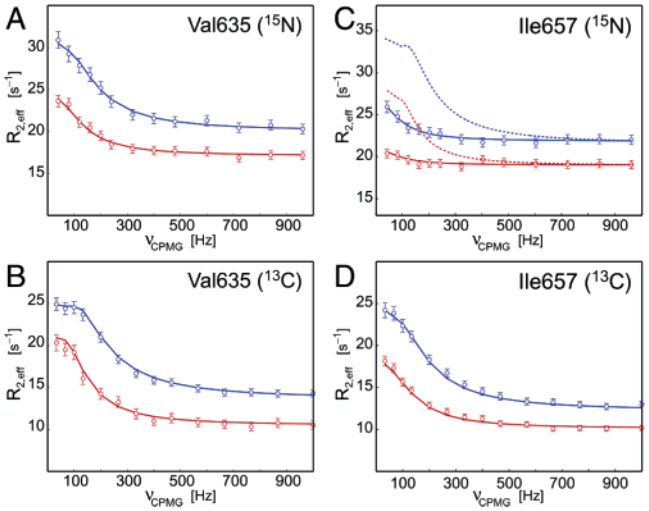

FIGURE 1: Representative backbone ^{15}N and side chain methyl ^{13}C relaxation dispersion profiles for Val635 (A and B) and Ile657 (C and D) of KIX [recorded at static magnetic field strengths of 18.8 (blue) and 11.7 T (red) at 20 °C], together with best-fit curves (—) obtained by combining the dispersions of all residues in a collective fit to a global two-site exchange model. ^{15}N and ^{13}C data were fit separately, yielding rate constants that are identical within uncertainties (for ^{15}N, $k_{GE} = 11 \pm 1$ s^{-1} and $k_{EG} = 310 \pm 20$ s^{-1}; for ^{13}C, $k_{GE} = 11 \pm 1$ s^{-1} and $k_{EG} = 270 \pm 30$ s^{-1}). For the backbone ^{15}N of Ile657, located in helix α3, hypothetical dispersion curves corresponding to complete unfolding (assuming random coil chemical shifts) are shown as dashed lines. Error bars represent uncertainties in relaxation rates.

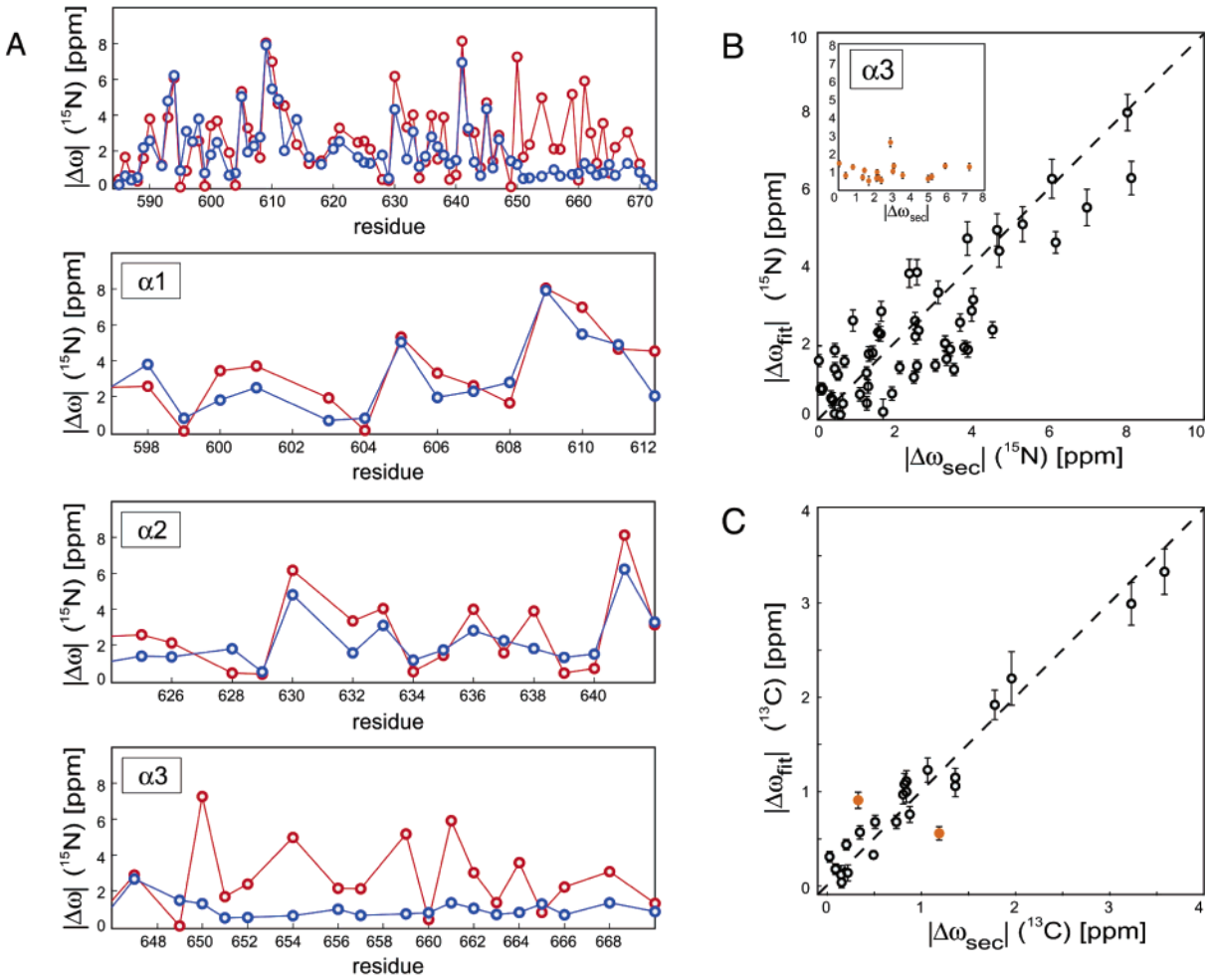

FIGURE 2: (A) Comparison of experimental backbone amide ^{15}N chemical shift changes upon the transition from G to E ($|\Delta\omega_{fit}|$, blue) and ^{15}N secondary chemical shifts ($|\Delta\omega_{sec}|$, red) as a function of residue number. (B) Correlation of $|\Delta\omega_{fit}|$ and $|\Delta\omega_{sec}|$ (^{15}N) for all residues except helix α3 (residues 646−669). The rmsd between $|\Delta\omega_{fit}|$ and $|\Delta\omega_{sec}|$ is 0.94 ppm, and the correlation coefficient, r, is 0.84. The inset shows data for helix α3 ($r = 0.06$). (C) Correlation of $|\Delta\omega_{fit}|$ and $|\Delta\omega_{sec}|$ for Val-γ, Leu-δ, and Ile-δ1 side chain methyl ^{13}C sites. The rmsd between $|\Delta\omega_{fit}|$ and $|\Delta\omega_{sec}|$ is 0.21 ppm, and $r = 0.96$. Data for side chain methyl ^{13}C sites of residues 657 and 660 that belong to helix α3 are colored orange. Excluding these two ^{13}C sites from the data reduces the rmsd to 0.18 ppm and increases r to 0.98.

on- or off-pathway) or cyclic mechanisms as described previously (*11*, *15*). The (very small) χ^2 reduction in three-state exchange models relative to the two-state model was assessed by *F*-test criteria, which show that introduction of a third state into the exchange model does not lead to statistically significant improvement of the fit at the 99% confidence level. Hence, we conclude that a simple two-state mechanism provides a self-consistent description of the microsecond-to-millisecond conformational exchange process of KIX under native conditions, and fitting the experimental dispersion profiles to a three-state mechanism is not justified.

It is worth mentioning that the fact that we find a two-state exchange process with these methods does not exclude the possibility of other conformational exchange processes within either state that are too fast to contribute to NMR line broadening. Most importantly, any additional fast ($<$10 μs) exchange process will manifest itself as a pre-equilibrium that leads to averaging of the chemical shifts of the interconverting species without affecting the extracted exchange rate constants for the observable two-state exchange process.

Persistent Structure in the High-Energy State of KIX. Structural (NMR chemical shift) information about high-energy state E is obtained from the relaxation dispersion data. Chemical shifts are determined by the local environment of individual nuclei and thus provide site-resolved information about protein structure. Figure 2 compares experimental backbone amide ^{15}N chemical shift changes that occur during the G → E transition, $|\Delta\omega_{fit}|$, and ^{15}N secondary chemical shifts $|\Delta\omega_{sec}|$, which were calculated as the difference between the chemical shift that is observed in the native state and tabulated random coil chemical shifts that would be expected for an unfolded conformation (*33*). For the majority of residues, including helices α1 and α2, the experimental values agree well with $|\Delta\omega_{sec}|$, indicating that the mechanism underlying the exchange broadening is consistent with unfolding of the polypeptide backbone. The rmsd between $|\Delta\omega_{fit}|$ and $|\Delta\omega_{sec}|$ is 0.94 ppm, which is similar to values obtained for complete unfolding of a Fyn SH3 domain mutant (D. M. Korzhnev, personal communication) and for unfolding of CspA from *E. coli* to a largely unstructured unfolded state (*40*), and reflects both the precision of experimental $|\Delta\omega_{fit}|$ values and uncertainties inherent to ^{15}N chemical shift predictions [backbone amide ^{15}N chemical shifts typically agree with experimental data with uncertainties on the order of 0.8−1.1 ppm (*33*, *41*)].

The situation is, however, strikingly different for helix α3. The conformational exchange contribution to the backbone

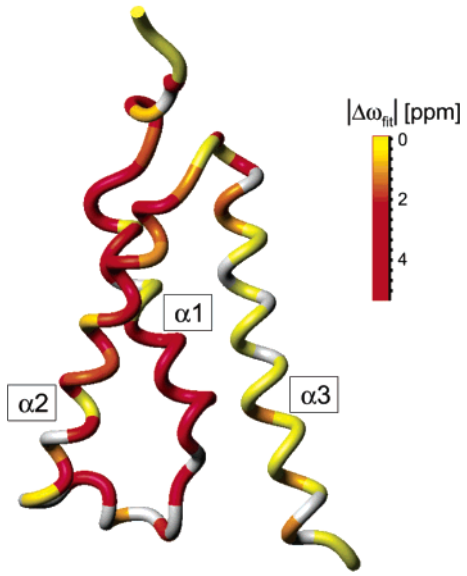

FIGURE 3: Backbone of KIX residues 586−672 [PDB entry 2AGH (*22*)] color-coded according to experimental ^{15}N chemical shift differences between the high-energy partially unfolded state and the native state, $|\Delta\omega_{fit}|$. Residues with a $|\Delta\omega_{fit}|$ of > 2 ppm are colored red, and residues with a $|\Delta\omega_{fit}|$ of 0 are colored yellow. For helix α3, all residues display uniformly low $|\Delta\omega_{fit}|$ values, whereas for the remainder of the backbone, $|\Delta\omega_{fit}|$ values range from ~0 to ~8 ppm and agree with secondary chemical shifts. Residues for which no ^{15}N experimental data are available are colored gray.

^{15}N line width in helix α3 is generally small, resulting in almost flat relaxation dispersion profiles for most residues (Figure 1C). In principle, small exchange contributions to the line width can result from only minor changes in resonance frequencies or, alternatively, if the time scale of the conformational exchange process involving helix α3 is outside the microsecond-to-millisecond regime. Of note, however, fitting only dispersion profiles for helix α3 to a global two-state exchange model yields rate constants for ^{15}N-labeled KIX at 27 °C ($k_{GE} = 17 \pm 1$ s^{-1} and $k_{EG} = 510 \pm 50$ s^{-1}) that are identical within experimental uncertainty to values obtained from a global fit, including all other residues in KIX ($k_{GE} = 17 \pm 1$ s^{-1} and $k_{EG} = 540 \pm 20$ s^{-1}). This verifies that ^{15}N sites in helix α3 sense the same kinetic process as the remainder of the protein backbone and can be included in the global fit. A comparison of experimental ^{15}N chemical shift changes that occur during the G → E transition with secondary chemical shifts for residues in helix α3 is shown in Figure 2A and in the inset of Figure 2B. With the exception of residue Asp647, which is located near the N-terminus of this helix, ^{15}N sites in helix α3 experience chemical shift changes in the global order-to-disorder transition that are considerably smaller than expected for unfolding, indicating that for these residues structure is retained in high-energy state E. Taken together, the backbone ^{15}N relaxation dispersion data demonstrate that for the bulk of residues, including helices α1 and α2, the transition from G to E is accompanied by a loss of local structure, resulting in chemical shifts that are very similar to values expected in the absence of local ordering, while an isolated element of secondary structure (helix α3) largely persists (Figure 3).

Hydrophobic Packing. To probe hydrophobic packing in the core of the KIX domain, ^{13}C single-quantum relaxation dispersion experiments were performed for methyl groups, providing site-specific measures of conformational exchange at side chain positions (*30*). KIX contains six Val, nine Leu, and three Ile residues, most of which participate in the formation of the hydrophobic core (*19*). Val-γ, Leu-δ, and Ile-δ1 methyl groups were selectively labeled with ^{13}C and ^{1}H in a ^{12}C and ^{2}H background using specifically labeled amino acid precursors (*26*, *27*). The relaxation dispersion profiles show that for methyl ^{13}C sites throughout the protein, including residues in stable helix α3, microsecond-to-millisecond conformational exchange significantly contributes to spin relaxation (Figure 1B,D). From 30 (of 33 Val-γ, Leu-δ, and Ile-δ1) sites that are not overlapped in two-dimensional ^{1}H−^{13}C correlation spectra, seven were identified for which $\chi_{glob}^2/\chi_{ind}^2 > 1.5$, indicating that microsecond-to-millisecond time scale motions other than the global G ↔ E transition contribute to the ^{13}C line width of these methyl groups (presumably involving aromatic side chains in the hydrophobic core) and are excluded from the analysis. A fit of the experimental data to a global two-site exchange model yields the following: $k_{GE} = 11 \pm 1$ s^{-1} and $k_{EG} = 270 \pm 30$ s^{-1} at 20 °C. While these rate constants differ from the values for the backbone-only ^{15}N-labeled sample of KIX because of the lower temperature used and the high level of deuteration in the methyl-labeled sample (*42*), they are identical to values determined independently from the backbone amide ^{15}N dispersion data obtained on the same (methyl-labeled) sample under identical conditions: $k_{GE} = 11 \pm 1$ s^{-1} and $k_{EG} = 310 \pm 20$ s^{-1} (Table 1). Thus, the hydrophobic core of the KIX domain is disrupted at the same rate as the backbone of the domain.

Table 1: Two-Site Conformational Exchange Parameters for the KIX Domain of CBP

sample	k_{GE}[a] (s^{-1})	k_{EG}[a] (s^{-1})	experiment
^{1}H[b] (27 °C)	17 ± 1	540 ± 20	^{15}N[c]
^{2}H[d] (20 °C)	11 ± 1	310 ± 20	^{15}N[c]
^{2}H[d] (20 °C)	11 ± 1	270 ± 30	^{13}C[e]

[a] k_{GE} and k_{EG} are the first-order rate constants for G → E and E → G transitions, respectively, obtained from global fits of the relaxation dispersion data. [b] Data for the uniformly ^{15}N labeled and protonated (^{1}H) sample, as described in Materials and Methods. [c] Rate constants obtained from backbone amide ^{15}N relaxation dispersion data. [d] Data for the selectively methyl labeled (^{13}C and ^{1}H) and uniformly ^{15}N labeled but otherwise deuterated (^{2}H) sample, as described in Materials and Methods. [e] Rate constants obtained from side chain methyl ^{13}C relaxation dispersion data.

Figure 2C compares experimental ^{13}C chemical shift changes that occur during the G → E transition, $|\Delta\omega_{fit}|$, and ^{13}C secondary chemical shifts, $|\Delta\omega_{sec}|$. The excellent correlation between $|\Delta\omega_{fit}|$ and $|\Delta\omega_{sec}|$ shows that ^{13}C chemical shifts in the high-energy partially unfolded form of KIX can be adequately modeled by canonical random coil chemical shifts. The better correlation between $|\Delta\omega_{fit}|$ and $|\Delta\omega_{sec}|$ for ^{13}C compared to ^{15}N chemical shifts (Figures 2B,C) reflects the fact that the precision of predicted ^{13}C random coil chemical shifts is considerably higher than for ^{15}N chemical shifts, which are more sensitive to external variables such as solvent and hydrogen bond effects (*34*). Of note, the observation that methyl ^{13}C chemical shifts in the high-energy form of KIX are uniformly close to chemical shifts of unstructured model peptides suggests that the hydrophobic core is devoid of specific tertiary interactions and precludes defined packing arrangements.

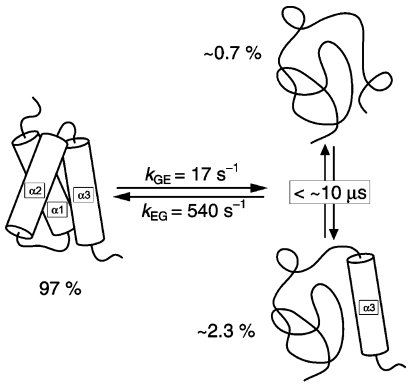

FIGURE 4: Conformational exchange scheme of KIX under native conditions, at pH 5.5 and 27 °C. The experimental data suggest a first-order conformational transition between the native ground state (left) that is populated to 97.0 ± 0.2% and a high-energy form (right) that is populated to 3.0 ± 0.2%. Thermodynamic data derived from native-state hydrogen exchange, urea denaturation, and relaxation dispersion experiments as well as NMR chemical shift data consistently indicate that within the high-energy form helix α3 is populated to ~75% while the completely unstructured (open) form of KIX is populated to ~25%. These values translate to total populations of 97.0, ~2.3, and ~0.7%, respectively.

Close inspection of Figure 2C reveals that the two methyl ^{13}C sites with the largest difference between $|\Delta\omega_{fit}|$ and $|\Delta\omega_{sec}|$ are Ile657-δ1 (the difference between $|\Delta\omega_{fit}|$ and $|\Delta\omega_{sec}|$ is 0.63 ppm) and Ile660-δ1 (the difference is 0.58 ppm), indicating that the local environment of these two methyl ^{13}C sites in the partially unfolded form of KIX may not be adequately represented by a random coil. These two methyl groups, which belong to helix α3, are embedded in a network of hydrophobic interactions within the core of the native KIX domain involving Leu607, Ile611, Val635, Ile657, and Ile660 side chains. However, since the only two residues that are affected belong to helix α3, we infer that local steric effects are responsible for this observation, consistent with the persistence of helix α3 in the partially unfolded form of KIX.

Exchange Model. Unfolding of KIX was followed by urea-induced denaturation by monitoring the CD signal at 222 nm, yielding an apparent free energy of unfolding of 2.9 ± 0.1 kcal/mol, which is significantly higher than the free energy difference of the G ↔ E conformational transition (2.1 ± 0.1 kcal/mol; see above). In addition, we performed native-state hydrogen exchange (NHX) experiments under equilibrium conditions. Only for four residues in KIX (Ala654, Ile657, Ile660, and Lys667) was backbone NH hydrogen exchange sufficiently slow to be measured by recording HSQC spectra, and all four residues are located in helix α3. This is in agreement with NMR relaxation dispersion results, which indicate that helices α1 and α2 (and the remainder of the protein backbone) are unprotected in the high-energy state (Figure 4). For these residues, ^{1}H−^{2}H exchange occurs with an observed rate constant k_{obs} that is equal to $K_{GE}k_{int}$, where k_{int} is the intrinsic ^{1}H−^{2}H exchange rate and K_{GE} is the equilibrium constant for the global G ↔ E conformational transition. For residues in helix α3, however, the observed ^{1}H−^{2}H rate constant is determined by the relation $k_{obs} = (K_{GE}K_{HEL})k_{int}$, where K_{HEL} is the equilibrium constant describing the opening of helix α3 within the partially unfolded form of KIX. For these residues, the apparent free energies (ΔG) calculated for the opening reaction of helix α3 as $-RT \ln(k_{obs}/k_{int})$ range from 2.5 to 3.2 kcal/mol and the average free energy is 2.8 ± 0.3 kcal/mol, in good agreement with the unfolding free energy that we measured by urea-induced denaturation (see above). Thus, the completely unstructured (open) form of KIX is ~0.7 kcal/mol less stable than the high-energy state that we have identified by NMR. This value corresponds to a K_{HEL} of ~0.3 or an ~75% population of helical structure within the high-energy state.

In principle, and contrary to equilibrium NHX experiments (*43*, *44*), pathway information on folding processes with more than two states can be obtained from relaxation dispersion data (*15*, *45*), because these experiments provide thermodynamic information (describing the equilibrium distribution of states) and kinetic information on *n*-state conformational exchange processes even though they are performed at thermodynamic equilibrium. For KIX, however, we are not obtaining mechanistic information beyond the description shown in Figure 4, because the formation of isolated helices is too fast to be observed by CPMG relaxation dispersion methods. Typically, isolated α-helices form in less than a microsecond (*46*), and such fast (<10 μs) processes do not result in sizable CPMG relaxation dispersion profiles (for ^{15}N nuclei and $\Delta\omega$ values that are typical for unfolding, up to 10 ppm). Rather, as any fast conformational exchange process does, a folding−unfolding transition of helix α3 efficiently averages chemical shifts. Thus, the $|\Delta\omega_{fit}|/|\Delta\omega_{sec}|$ ratio provides a measure of the population of helical structure within the high-energy form. On the basis of residues that have significant (>3 ppm) ^{15}N secondary chemical shifts (Figure 2A), we estimate that the lower limit of helical content for helix α3 is ~70%, in agreement with the urea denaturation and the NHX data.

To probe the disruption of residual structure in the partially unfolded form of KIX upon chemical denaturation, we performed backbone amide ^{15}N relaxation dispersion experiments at various low (≤1.5 M) urea concentrations. The data were fit to a global two-site exchange model (G ↔ E) as described above, and changes in site-specific chemical shift changes upon unfolding, $|\Delta\omega_{fit}|$, were monitored (Figure 5). Only for residues in helix α3 (Tyr650, Ala654, Lys659, and Gln661) did values of $|\Delta\omega_{fit}|$ increase measurably upon addition of urea, consistent with a disruption of residual helical structure and a decrease of the population of helix α3 within the high-energy form of KIX, while for all other residues, values of $|\Delta\omega_{fit}|$ remain invariant with protein concentration.

Taken together, all experimental data are consistent with a first-order conformational transition between folded ground state G and high-energy form E that is populated to 3.0 ± 0.2% at 27 °C and pH 5.5. NMR chemical shift data and thermodynamic data derived from NHX, urea denaturation, and relaxation dispersion experiments consistently indicate that within the high-energy form helix α3 is populated at equilibrium to ~75%, while the completely unstructured form of KIX is populated to ~25%. Data obtained at different urea concentrations suggest that within the high-energy form of KIX the population of helix α3 decreases when chemical denaturant is added.

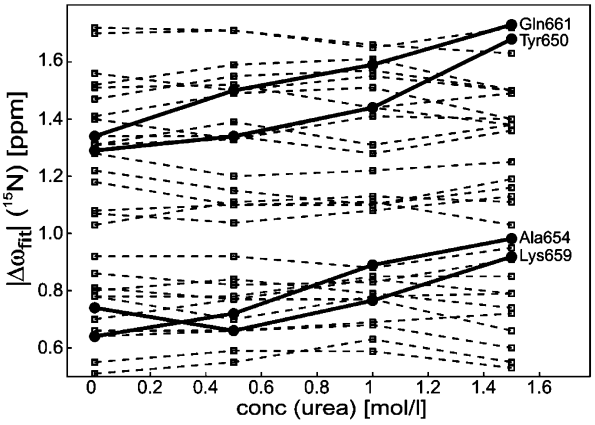

FIGURE 5: Experimental backbone amide ^{15}N chemical shift changes upon the transition from G to E, $|\Delta\omega_{fit}|$, as a function of urea concentration. Data for the four residues in helix α3 with a $|\Delta\omega_{sec}|$ of >4.0 ppm (Tyr650, Ala654, Lys659, and Gln661) are displayed as circles and lines, while data for all residues outside helix α3 (where 0.5 ppm < $|\Delta\omega_{fit}|$ < 1.8 ppm) are displayed as squares and dashed lines. The $|\Delta\omega_{fit}|$ values were obtained from global fits.

DISCUSSION

The NMR relaxation dispersion data for the KIX domain of CBP show that under nondenaturing conditions this protein permanently exchanges between its folded (native) ground state and a high-energy state that is populated to 3.0 ± 0.2% at 27 °C and pH 5.5, in an apparent two-state manner. All NMR spectroscopic probes in the protein experience the same kinetic transition between the two states, in line with a cooperative first-order conformational transition. Additional support for a two-state mechanism is provided by comparison of backbone amide (^{15}N) and side chain methyl (^{13}C) relaxation dispersion data, which clearly demonstrate that the hydrophobic core of KIX is disrupted at the same rate as the backbone of the domain. The chemical shift data provide a picture of the sparsely populated high-energy state as a partially unfolded form of the protein that contains residual secondary structure around residues 646−669, which corresponds to helix α3, while the remainder of the backbone is unstructured. Both relaxation dispersion and native-state hydrogen exchange results suggest a population of ∼75% for helix α3 within the high-energy state. In addition, the side chain relaxation dispersion data show that this partially unfolded form of KIX lacks specific tertiary interactions and rigid hydrophobic packing.

Weakly populated partially unfolded forms represent a significant feature of the energy landscapes of proteins under native conditions as high-energy states that are accessible to the polypeptide chain and may well be of biological importance. Disordered regions of proteins confer considerable functional advantage on proteins, as they allow efficient interaction with binding partners and provide a mechanism for the regulation of cellular processes. For example, the presence of locally disordered segments in a protein can play an important role in ligand binding and in molecular recognition, as many disordered regions fold on binding to their targets (*18*, *47*). Coupled folding and binding is accompanied by a considerable decrease in conformational entropy, which facilitates the formation of a complex with high specificity yet relatively low affinity (and therefore high reversibility) by enthalpy−entropy compensation. These features are fundamentally important for regulatory processes and signal transduction, which require reversible and highly specific binding of biological targets (*48*). The low thermodynamic stability of the KIX domain of CBP might be relevant for the affinity with which it binds its target domains, and the high degree of conformational flexibility in the high-energy form of KIX could be related to its versatility in interacting with a wide range of target molecules.

In addition, partially unfolded forms of proteins can represent intermediate states that are transiently populated in protein folding processes (*4*). In a recent stopped-flow kinetic study of a similar KIX domain construct employing urea denaturation, a folding intermediate was indeed identified by observation of a significant unresolved amplitude (burst phase) as well as a rollover in chevron plots (*49*). It was concluded that KIX folds by a three-state mechanism, involving the very rapid formation of a compact intermediate within the dead time of the stopped-flow instrument (∼3.5 ms), followed by a second, much slower event to form the native state. Our NMR results obtained under nondenaturing conditions are consistent with apparent two-state kinetics, with unfolding and folding rates (k_{GE} = 17 ± 1 s^{-1} and k_{EG} = 540 ± 20 s^{-1} at pH 5.5, 25 mM NaCl, and 27 °C) very similar to the values that were estimated for the slower kinetic phase in the stopped-flow experiments at pH 7.5 and 25 °C [∼30 and ∼300 s^{-1}, respectively (*49*)] and pH 6.0 and 25 °C (Supporting Information of ref *49*).

How can we reconcile these observations? Under native conditions, the partially unfolded form of KIX contains persistent structure, helix α3. NMR relaxation dispersion experiments performed at various urea concentrations indicate a progressive loss of residual structure, suggesting that helix α3 is disrupted in the partially unfolded state when chemical denaturant is added. One possible model that reconciles chemical denaturation (stopped-flow) data and equilibrium (NMR relaxation dispersion) results is one in which, starting from the urea-denatured state in chemical denaturation experiments, helix α3 is formed first, within the dead time of the stopped-flow instrument, and the slower kinetic phase corresponds to the process that we observe by NMR. Within that model, the weakly populated high-energy form of KIX that we have characterized here would correspond to the folding intermediate that transiently accumulates in denaturant-induced refolding experiments. Notably, it has been demonstrated for various proteins that similar partially unfolded forms detected by hydrogen exchange experiments can represent equilibrium analogues of kinetic folding intermediates (*50*−*52*). Indeed, the structure of the high-energy form of KIX bears a remarkable resemblance to folding intermediates that have been observed for other proteins. Folding intermediates typically represent partially unfolded forms of proteins containing significant (secondary) structure and variable degrees of conformational heterogeneity (*3*, *11*, *50*−*56*).

The persistence of stable secondary structure in an otherwise unstructured background is compatible with a hierarchic (framework) folding process, in which folding begins with the formation of local secondary structure without requiring specific tertiary interactions, followed by docking of structural elements to form the native tertiary structure (*57*, *58*). Hierarchic folding mechanisms require

secondary structure to be inherently stable, and the inherent stabilities of α-helices can have a measurable effect on the apparent folding mechanism (*59*). It has been demonstrated that within a family of topologically related proteins, folding proceeds through increasingly populated helical intermediates as the intrinsic helical propensity increases (*60*). Likewise, increasing the helical stability by mutation can stabilize partially unfolded helical intermediates and switch the apparent folding mechanism from a two-state model to a three-state model (*61*, *62*).

For the partially unfolded form of KIX, the experimental observation of a strong conformational preference for helix α3 agrees well with helical propensities calculated using the AGADIR helix−coil prediction algorithm (*63*). Helix α3 is indeed predicted to have a high propensity for formation (63% averaged over all residues), ∼50 and ∼10 times higher than those for helices α1 and α2, respectively (see the Supporting Information). Intriguingly, numerous proteins have been shown to fold by stepwise assembly of independent cooperative folding−unfolding units (foldons), and such foldons tend to be coincident with secondary structural elements (*56*). The relaxation dispersion data provide no information, however, about the order of events involving the formation of helices α1 and α2 as folding progresses to the native structure. Additional studies will be necessary to determine whether folding indeed proceeds in a stepwise manner where helices α1 and α2 (and the two short 3_{10}-helices) form separately before docking to establish the native tertiary structure or whether the hydrophobic residues located in helix α3 constitute a folding nucleus around which the remainder of the structure consolidates.

CONCLUDING REMARKS

High-energy states of proteins are routinely characterized employing native-state hydrogen exchange experiments that report on the presence (or absence) of hydrogen-bonded structure or burial at the level of individual residues and on thermodynamic stabilities of persistent structure (*4*, *5*). Relaxation dispersion techniques ideally complement NHX experiments by providing site-specific kinetic information and pathway information along with chemical shift information about high-energy forms, in favorable cases when the conformational transition occurs on a microsecond-to-millisecond time scale and the high-energy form is sufficiently populated (to ∼1% or more). Moreover, relaxation dispersion experiments are not restricted to solvent exchange-labile sites within proteins, facilitating the investigation of specific structural aspects, including the formation of the hydrophobic core. The amount and diversity of the structural information that can be obtained for high-energy forms (and folding intermediates) under native conditions will further increase in the future as novel isotope labeling patterns for proteins are becoming available.

ACKNOWLEDGMENT

We are grateful to Alanna Schepartz (Yale University, New Haven, CT) for generously providing the pHisKIX expression vector.

SUPPORTING INFORMATION AVAILABLE

A figure showing predicted α-helical propensities for the KIX domain using AGADIR. This material is available free of charge via the Internet at http://pubs.acs.org.

REFERENCES

1. Shortle, D. (1996) The denatured state (the other half of the folding equation) and its role in protein stability, *FASEB J. 10*, 27−34.
2. Crowhurst, K. A., and Forman-Kay, J. D. (2003) Aromatic and methyl NOEs highlight hydrophobic clustering in the unfolded state of an SH3 domain, *Biochemistry 42*, 8687−8695.
3. Religa, T. L., Markson, J. S., Mayor, U., Freund, S. M., and Fersht, A. R. (2005) Solution structure of a protein denatured state and folding intermediate, *Nature 437*, 1053−1056.
4. Englander, S. W. (2000) Protein folding intermediates and pathways studied by hydrogen exchange, *Annu. Rev. Biophys. Biomol. Struct. 29*, 213−238.
5. Krishna, M. M., Hoang, L., Lin, Y., and Englander, S. W. (2004) Hydrogen exchange methods to study protein folding, *Methods 34*, 51−64.
6. Bai, Y., Chung, J., Dyson, H. J., and Wright, P. E. (2001) Structural and dynamic characterization of an unfolded state of poplar apoplastocyanin formed under nondenaturing conditions, *Protein Sci. 10*, 1056−1066.
7. Mayor, U., Grossmann, J. G., Foster, N. W., Freund, S. M., and Fersht, A. R. (2003) The denatured state of engrailed homeodomain under denaturing and native conditions, *J. Mol. Biol. 333*, 977−991.
8. Chugha, P., Sage, H. J., and Oas, T. G. (2006) Methionine oxidation of monomeric λ repressor: The denatured state ensemble under nondenaturing conditions, *Protein Sci. 15*, 533−542.
9. Myers, J. K., and Oas, T. G. (2002) Mechanism of fast protein folding, *Annu. Rev. Biochem. 71*, 783−815.
10. Palmer, A. G., III, Kroenke, C. D., and Loria, J. P. (2001) Nuclear magnetic resonance methods for quantifying microsecond-to-millisecond motions in biological macromolecules, *Methods Enzymol. 339*, 204−238.
11. Korzhnev, D. M., Salvatella, X., Vendruscolo, M., Di Nardo, A. A., Davidson, A. R., Dobson, C. M., and Kay, L. E. (2004) Low-populated folding intermediates of Fyn SH3 characterized by relaxation dispersion NMR, *Nature 430*, 586−590.
12. Korzhnev, D. M., Neudecker, P., Mittermaier, A., Orekhov, V. Y., and Kay, L. E. (2005) Multiple-site exchange in proteins studied with a suite of six NMR relaxation dispersion experiments: An application to the folding of a Fyn SH3 domain mutant, *J. Am. Chem. Soc. 127*, 15602−15611.
13. Choy, W. Y., Zhou, Z., Bai, Y., and Kay, L. E. (2005) An ^{15}N NMR spin relaxation dispersion study of the folding of a pair of engineered mutants of apocytochrome b_{562}, *J. Am. Chem. Soc. 127*, 5066−5072.
14. Grey, M. J., Tang, Y., Alexov, E., McKnight, C. J., Raleigh, D. P., and Palmer, A. G., III (2006) Characterizing a partially folded intermediate of the villin headpiece domain under non-denaturing conditions: Contribution of His41 to the pH-dependent stability of the N-terminal subdomain, *J. Mol. Biol. 355*, 1078−1094.
15. Mittermaier, A., Korzhnev, D. M., and Kay, L. E. (2005) Side-chain interactions in the folding pathway of a Fyn SH3 domain mutant studied by relaxation dispersion NMR spectroscopy, *Biochemistry 44*, 15430−15436.
16. Goodman, R. H., and Smolik, S. (2000) CBP/p300 in cell growth, transformation, and development, *Genes Dev. 14*, 1553−1577.
17. Giordano, A., and Avantaggiati, M. L. (1999) p300 and CBP: Partners for life and death, *J. Cell. Physiol. 181*, 218−230.
18. Dyson, H. J., and Wright, P. E. (2005) Intrinsically unstructured proteins and their functions, *Nat. Rev. Mol. Cell Biol. 6*, 197−208.
19. Radhakrishnan, I., Perez-Alvarado, G. C., Parker, D., Dyson, H. J., Montminy, M. R., and Wright, P. E. (1997) Solution structure of the KIX domain of CBP bound to the transactivation domain of CREB: A model for activator:coactivator interactions, *Cell 91*, 741−752.
20. Zor, T., De Guzman, R. N., Dyson, H. J., and Wright, P. E. (2004) Solution structure of the KIX domain of CBP bound to the transactivation domain of c-Myb, *J. Mol. Biol. 337*, 521−534.
21. Campbell, K. M., and Lumb, K. J. (2002) Structurally distinct modes of recognition of the KIX domain of CBP by Jun and CREB, *Biochemistry 41*, 13956−13964.
22. De Guzman, R. N., Goto, N. K., Dyson, H. J., and Wright, P. E. (2006) Structural basis for cooperative transcription factor binding to the CBP coactivator, *J. Mol. Biol. 355*, 1005−1013.
23. Goto, N. K., Zor, T., Martinez-Yamout, M., Dyson, H. J., and Wright, P. E. (2002) Cooperativity in transcription factor binding to the coactivator CREB-binding protein (CBP). The mixed lineage

leukemia protein (MLL) activation domain binds to an allosteric site on the KIX domain, *J. Biol. Chem. 277*, 43168−43174.
24. Ernst, P., Wang, J., Huang, M., Goodman, R. H., and Korsmeyer, S. J. (2001) MLL and CREB bind cooperatively to the nuclear coactivator CREB-binding protein, *Mol. Cell. Biol. 21*, 2249−2258.
25. Rutledge, S. E., Volkman, H. M., and Schepartz, A. (2003) Molecular recognition of protein surfaces: High affinity ligands for the CBP KIX domain, *J. Am. Chem. Soc. 125*, 14336−14347.
26. Goto, N. K., Gardner, K. H., Mueller, G. A., Willis, R. C., and Kay, L. E. (1999) A robust and cost-effective method for the production of Val, Leu, Ile (δ1) methyl-protonated ^{15}N-, ^{13}C-, ^{2}H-labeled proteins, *J. Biomol. NMR 13*, 369−374.
27. Lichtenecker, R., Ludwiczek, M. L., Schmid, W., and Konrat, R. (2004) Simplification of protein NOESY spectra using bioorganic precursor synthesis and NMR spectral editing, *J. Am. Chem. Soc. 126*, 5348−5349.
28. Loria, J. P., Rance, M., and Palmer, A. G., III (1999) A relaxation-compensated Carr-Purcell-Meiboom-Gill sequence for characterizing chemical exchange by NMR spectroscopy, *J. Am. Chem. Soc. 121*, 2331−2332.
29. Tollinger, M., Skrynnikov, N. R., Mulder, F. A. A., Forman-Kay, J. D., and Kay, L. E. (2001) Slow dynamics in folded and unfolded states of an SH3 domain, *J. Am. Chem. Soc. 123*, 11341−11352.
30. Skrynnikov, N. R., Mulder, F. A., Hon, B., Dahlquist, F. W., and Kay, L. E. (2001) Probing slow time scale dynamics at methyl-containing side chains in proteins by relaxation dispersion NMR measurements: Application to methionine residues in a cavity mutant of T4 lysozyme, *J. Am. Chem. Soc. 123*, 4556−4566.
31. McConnell, H. M. (1958) Reaction rates by nuclear magnetic resonance, *J. Chem. Phys. 28*, 430−431.
32. Motulsky, H., and Christopoulos, A. (2004) *Fitting Models to Biological Data using Linear and Nonlinear Regression*, Oxford University Press, Oxford, U.K.
33. Schwarzinger, S., Kroon, G. J., Foss, T. R., Chung, J., Wright, P. E., and Dyson, H. J. (2001) Sequence-dependent correction of random coil NMR chemical shifts, *J. Am. Chem. Soc. 123*, 2970−2978.
34. Wishart, D. S., Bigam, C. G., Holm, A., Hodges, R. S., and Sykes, B. D. (1995) ^{1}H, ^{13}C and ^{15}N random coil NMR chemical shifts of the common amino acids. I. Investigations of nearest-neighbor effects, *J. Biomol. NMR 5*, 67−81.
35. Bai, Y., Milne, J. S., Mayne, L., and Englander, S. W. (1993) Primary structure effects on peptide group hydrogen exchange, *Proteins 17*, 75−86.
36. Pace, C. N., and Shaw, K. L. (2000) Linear extrapolation method of analyzing solvent denaturation curves, *Proteins Suppl. 4*, 1−7.
37. Maxwell, K. L., Wildes, D., Zarrine-Afsar, A., De Los Rios, M. A., Brown, A. G., Friel, C. T., Hedberg, L., Horng, J. C., Bona, D., Miller, E. J., Vallee-Belisle, A., Main, E. R., Bemporad, F., Qiu, L., Teilum, K., Vu, N. D., Edwards, A. M., Ruczinski, I., Poulsen, F. M., Kragelund, B. B., Michnick, S. W., Chiti, F., Bai, Y., Hagen, S. J., Serrano, L., Oliveberg, M., Raleigh, D. P., Wittung-Stafshede, P., Radford, S. E., Jackson, S. E., Sosnick, T. R., Marqusee, S., Davidson, A. R., and Plaxco, K. W. (2005) Protein folding: Defining a "standard" set of experimental conditions and a preliminary kinetic data set of two-state proteins, *Protein Sci. 14*, 602−616.
38. Farrow, N. A., Muhandiram, R., Singer, A. U., Pascal, S. M., Kay, C. M., Gish, G., Shoelson, S. E., Pawson, T., Forman-Kay, J. D., and Kay, L. E. (1994) Backbone dynamics of a free and phosphopeptide-complexed Src homology 2 domain studied by ^{15}N NMR relaxation, *Biochemistry 33*, 5984−6003.
39. Korzhnev, D. M., Skrynnikov, N. R., Millet, O., Torchia, D. A., and Kay, L. E. (2002) An NMR experiment for the accurate measurement of heteronuclear spin-lock relaxation rates, *J. Am. Chem. Soc. 124*, 10743−10753.
40. Kloiber, K., Tollinger, M., and Konrat, R. Manuscript in preparation.
41. Braun, D., Wider, G., and Wuthrich, K. (1994) Sequence-corrected ^{15}N 'Random Coil' Chemical Shifts, *J. Am. Chem. Soc. 116*, 8466−8469.
42. Brockwell, D., Yu, L., Cooper, S., McCleland, S., Cooper, A., Attwood, D., Gaskell, S. J., and Barber, J. (2001) Physicochemical consequences of the perdeuteriation of glutathione S-transferase from *S. japonicum*, *Protein Sci. 10*, 572−580.
43. Clarke, J., and Fersht, A. R. (1996) An evaluation of the use of hydrogen exchange at equilibrium to probe intermediates on the protein folding pathway, *Folding Des. 1*, 243−254.
44. Clarke, J., Itzhaki, L. S., and Fersht, A. R. (1997) Hydrogen exchange at equilibrium: A short cut for analysing protein-folding pathways? *Trends Biochem. Sci. 22*, 284−287.
45. Mittermaier, A., and Kay, L. E. (2006) New tools provide new insights in NMR studies of protein dynamics, *Science 312*, 224−228.
46. Eaton, W. A., Munoz, V., Thompson, P. A., Henry, E. R., and Hofrichter, J. (1998) Kinetics and Dynamics of Loops, α-Helices, β-Hairpins and Fast Folding Proteins, *Acc. Chem. Res. 31*, 745−753.
47. Tompa, P. (2005) The interplay between structure and function in intrinsically unstructured proteins, *FEBS Lett. 579*, 3346−3354.
48. Iakoucheva, L. M., Brown, C. J., Lawson, J. D., Obradovic, Z., and Dunker, A. K. (2002) Intrinsic disorder in cell-sgnalling and cancer-associated proteins, *J. Mol. Biol. 323*, 573−584.
49. Horng, J. C., Tracz, S. M., Lumb, K. J., and Raleigh, D. P. (2005) Slow folding of a three-helix protein via a compact intermediate, *Biochemistry 44*, 627−634.
50. Mayor, U., Guydosh, N. R., Johnson, C. M., Grossmann, J. G., Sato, S., Jas, G. S., Freund, S. M., Alonso, D. O., Daggett, V., and Fersht, A. R. (2003) The complete folding pathway of a protein from nanoseconds to microseconds, *Nature 421*, 863−867.
51. Raschke, T. M., and Marqusee, S. (1997) The kinetic folding intermediate of ribonuclease H resembles the acid molten globule and partially unfolded molecules detected under native conditions, *Nat. Struct. Biol. 4*, 298−304.
52. Bai, Y., Sosnick, T. R., Mayne, L., and Englander, S. W. (1995) Protein folding intermediates: Native-state hydrogen exchange, *Science 269*, 192−197.
53. Gsponer, J., Hopearuoho, H., Whittaker, S. B., Spence, G. R., Moore, G. R., Paci, E., Radford, S. E., and Vendruscolo, M. (2006) Determination of an ensemble of structures representing the intermediate state of the bacterial immunity protein Im7, *Proc. Natl. Acad. Sci. U.S.A. 103*, 99−104.
54. Krishna, M. M., Lin, Y., Mayne, L., and Englander, S. W. (2003) Intimate view of a kinetic protein folding intermediate: residue-resolved structure, interactions, stability, folding and unfolding rates, homogeneity, *J. Mol. Biol. 334*, 501−513.
55. Jennings, P. A., and Wright, P. E. (1993) Formation of a molten globule intermediate early in the kinetic folding pathway of apomyoglobin, *Science 262*, 892−896.
56. Maity, H., Maity, M., Krishna, M. M., Mayne, L., and Englander, S. W. (2005) Protein folding: The stepwise assembly of foldon units, *Proc. Natl. Acad. Sci. U.S.A. 102*, 4741−4746.
57. Kim, P. S., and Baldwin, R. L. (1982) Specific intermediates in the folding reactions of small proteins and the mechanism of protein folding, *Annu. Rev. Biochem. 51*, 459−489.
58. Baldwin, R. L., and Rose, G. D. (1999) Is protein folding hierarchic? I. Local structure and peptide folding, *Trends Biochem. Sci. 24*, 26−33.
59. Daggett, V., and Fersht, A. R. (2003) Is there a unifying mechanism for protein folding? *Trends Biochem. Sci. 28*, 18−25.
60. Gianni, S., Guydosh, N. R., Khan, F., Caldas, T. D., Mayor, U., White, G. W., DeMarco, M. L., Daggett, V., and Fersht, A. R. (2003) Unifying features in protein-folding mechanisms, *Proc. Natl. Acad. Sci. U.S.A. 100*, 13286−13291.
61. White, G. W., Gianni, S., Grossmann, J. G., Jemth, P., Fersht, A. R., and Daggett, V. (2005) Simulation and experiment conspire to reveal cryptic intermediates and a slide from the nucleation-condensation to framework mechanism of folding, *J. Mol. Biol. 350*, 757−775.
62. Cranz-Mileva, S., Friel, C. T., and Radford, S. E. (2005) Helix stability and hydrophobicity in the folding mechanism of the bacterial immunity protein Im9, *Protein Eng., Des. Sel. 18*, 41−50.
63. Lacroix, E., Viguera, A. R., and Serrano, L. (1998) Elucidating the folding problem of α-helices: Local motifs, long-range electrostatics, ionic-strength dependence and prediction of NMR parameters, *J. Mol. Biol. 284*, 173−191.

BI0607305